Molecular simulation of transport in nanopores: Application of the transient-time correlation function formalism

Caroline Desgranges and Jerome Delhommelle
Department of Chemical Engineering, University of South Carolina, 301 Main Street, Columbia, South Carolina 29208, USA
(Received 30 October 2007; published 19 February 2008)

We report on nonequilibrium molecular dynamics (NEMD) simulation results on the color conductivity of fluids confined in cylindrical nanopores. Because conventional NEMD methods are restricted to fields several orders of magnitude stronger than those accessible by experiment, these methods have provided access so far only to the response of the fluid under far-from-equilibrium conditions. Using the transient-time correlation function formalism, we show how NEMD simulations can be extended to study the conductivity of a model liquid confined in a cylindrical nanopore and subjected to an arbitrarily low (and realistic) field. Our results provide a full picture of the dependence of conductivity on the applied field and on the effective diameter of the nanopore. They also demonstrate that the conductivity steadily increases—up to twice the value evaluated for the bulk—as the effective radius of the pore decreases.

DOI: 10.1103/PhysRevE.77.027701 PACS number(s): 02.70.Ns, 66.10.−x, 82.20.Wt

Understanding the transport of ions through nanoscopic pores is essential for many scientific and technological applications such as, e.g., the ionic permeation of zeolites, carbon nanotubes, and ion channels through cell membranes [1–4]. Nonequilibrium molecular dynamics (NEMD) simulations provide a direct access to the microscopic structural changes induced by the applied field. It is therefore a valuable tool for understanding how the structure and the transport properties of liquids are affected by the external field. However, conventional NEMD methods allow study only of systems subjected to very strong fields, typically of the order of 10^9 V m^{-1} [5,6], i.e., several orders of magnitude larger than the experimentally accessible rates. Therefore, these methods provide insight into the response of the fluid only under far-from-equilibrium conditions. The limitation to very strong fields directly stems from the conventional NEMD method. In conventional NEMD simulations, properties are averaged over the steady state. For weak fields, the signal-to-noise ratio is very small: the steady-state response becomes very noisy and the steady-state averages are essentially impossible to analyze. Having a large signal-to-noise ratio (and hence subjecting the fluid to very strong fields) is crucial to obtain meaningful averages in the steady state. This basically prevents the nonequilibrium response from being accessed for realistic values of the field. Therefore, a direct comparison between simulation and experiment still remains impossible.

The aim of this work is to address the inability of conventional NEMD methods to study the response of a liquid subjected to experimentally accessible fields. For this purpose, we consider the transient-time correlation function (TTCF) formalism [7–10]. The TTCF formalism is essentially a nonlinear generalization of the Green-Kubo relations. Although this formalism is fairly general, applications of the TTCF approach have been restricted so far to the determination of the viscosity of simple fluids at low shear rates [11–14], to simple liquids undergoing elongational flow [15], and, more recently, to the viscosity of decane [16] and the electric conductivity of molten sodium chloride [17]. In this work, we show how the TTCF approach can be applied to determine the conductivity of a fluid confined in a nanopore and subjected to a realistic field.

From a practical point of view, application of the TTCF method consists in monitoring the response of the system over a large number of nonequilibrium trajectories. For that purpose, we generate many equilibrium configurations during the course of a long equilibrium trajectory (governed by Newton's equations of motion). Each of these configurations is the starting point for a nonequilibrium trajectory. The nonequilibrium trajectory is generated by subjecting the fluid to a color field $\mathbf{E}$ along the x direction. Color fields have been used to understand phase transitions in strongly driven systems (such as colloidal mixtures [18]) and transport (through the evaluation of the color conductivity) in recent years. During both the equilibrium and nonequilibrium trajectories, the temperature of the system is fixed by adding a thermostatting term to the equations of motion. Using a thermostat for the whole confined fluid relies on the assumption that, when the confined fluid is subjected to an external field, no significant temperature gradient develops across the confined fluid. The essentially flat temperature profiles observed in previous work [19–21] support this approximation. We expect even flatter temperature profiles for the very weak fields studied in this work with the TTCF approach. The choice of a specific thermostatting method may have a significant effect on the results obtained during the nonequilibrium trajectories [22–25]. Most thermostats fix the value taken by a kinetic expression for the temperature defined from an *ad hoc* version of the equipartition theorem [5,6]. In this expression, the temperature is evaluated from the streaming kinetic energy, i.e., the kinetic energy relative to the flow of each species. Any inaccuracy in the determination of the flow velocities may result in inaccuracies in the calculated current and conductivity. Recent work has shown that this problem can be circumvented by using a configurational thermostat [26–31] based on a purely configurational expression for the temperature [32,33].

The equations of motion for the nonequilibrium trajectories are defined as follows:

$$\dot{\mathbf{r}}_i = \frac{\mathbf{p}_i}{m} - \eta \nabla_i \Phi,$$

$$\dot{\mathbf{p}}_i = -\nabla_i \Phi + z_i \mathbf{E},$$

$$\dot{\eta} = \frac{1}{Q_\eta}\left(N\sum_{i=1}^{N} (\nabla_i \Phi)^2 - k_B T \sum_{i=1}^{N} \nabla_i^2 \Phi \right), \tag{1}$$

in which $\mathbf{r}_i$, $\mathbf{p}_i$, m, and z_i denote the position, momentum, mass, and charge of particle i, $\mathbf{E}$ the color field (collinear to the x axis), Φ the potential energy of the system, k_B Boltzmann's constant, T the target value for the temperature, and η an additional dynamical variable which plays the role of a friction coefficient. Q_η can be thought of as the mass associated with the heat bath. The equations of motion for the equilibrium trajectories can be recovered by simply setting $\mathbf{E}=\mathbf{0}$. This thermostat fixes the configurational temperature T_{conf} defined as $k_B T_{\text{conf}} = \langle \Sigma_{i=1}^{N} (\nabla_i \Phi)^2 \rangle / \langle \Sigma_{i=1}^{N} \nabla_i^2 \Phi \rangle$ to the target value. As shown by Braga and Travis [30], these equations of motion generate the canonical distribution.

We now briefly outline the general derivation proposed by Evans and Morriss [10] to show how it can be applied to a fluid following the equations of motion given by Eq. (1). Let us consider a phase variable $B(\mathbf{\Gamma})$, where $\mathbf{\Gamma}$ denotes a phase space point. In the Heisenberg representation, the average of B at time t is $\langle B(t) \rangle = \int d\mathbf{\Gamma}\, f(0) B(\mathbf{\Gamma}; t)$, where $f(0)$ is the initial distribution function. If we differentiate this expression with respect to time, we obtain, for time-independent external fields,

$$\frac{d\langle B(t) \rangle}{dt} = \int d\mathbf{\Gamma}\, f(0) \frac{d\mathbf{\Gamma}}{dt} \frac{\partial B(t)}{\partial \mathbf{\Gamma}}. \tag{2}$$

By integrating by parts and realizing that the boundary term vanishes in periodic systems [10], we see that

$$\frac{d\langle B(t) \rangle}{dt} = -\int d\mathbf{\Gamma}\, B(t) \frac{\partial}{\partial \mathbf{\Gamma}} \frac{d\mathbf{\Gamma}}{dt} f(0). \tag{3}$$

Finally, integrating with respect to time, we obtain the nonlinear nonequilibrium response

$$\langle B(t) \rangle = \langle B(0) \rangle - \int_0^t ds \int d\mathbf{\Gamma} B(s) \frac{\partial}{\partial \mathbf{\Gamma}} \cdot \frac{d\mathbf{\Gamma}}{dt} f(0) \tag{4}$$

If the initial distribution is canonical and if the dynamics of the system follows Eq. (1), then, to the first order [10],

$$\frac{\partial}{\partial \mathbf{\Gamma}} \left(f(0) \frac{d\mathbf{\Gamma}}{dt} \right) = f(0) \left[\frac{\partial \dot{\mathbf{\Gamma}}}{\partial \mathbf{\Gamma}} + \dot{\mathbf{\Gamma}} \cdot \frac{\partial}{\partial \mathbf{\Gamma}} \left(\frac{-H_0(\mathbf{\Gamma})}{k_B T} \right) \right]$$

$$= f(0) \left(-\frac{V}{k_B T} \sum_{i=1}^{N} \frac{\mathbf{E} \cdot \mathbf{p}_i}{m} \right), \tag{5}$$

where $H_0 = \Sigma_{i=1}^{N} \mathbf{p}_i^2/(2m) + \Phi + Q_\eta \eta^2/2$ is the Hamiltonian of the extended system. Since $\mathbf{E}$ is collinear to the x axis, we define the color current along the x axis as $J_x = \Sigma_{i=1}^{N} z_i \mathbf{p}_i / mV$, where V is the volume accessible to the confined fluid. The average of B at time t is given by

$$\langle B(t) \rangle = \langle B(0) \rangle + \frac{VE}{k_B T} \int_0^t \langle B(s) J_x(0) \rangle ds. \tag{6}$$

If we choose $B(t) = J_x(t)$, the equilibrium average $\langle J_x(0) \rangle$ is equal to 0 and we obtain the following expression for $\langle J_x(t) \rangle$:

$$\langle J_x(t) \rangle = \frac{VE}{k_B T} \int_0^t \langle J_x(s) J_x(0) \rangle ds. \tag{7}$$

It is then straightforward to evaluate the color conductivity according to

$$\langle \sigma(t) \rangle = \frac{V}{k_B T} \int_0^t \langle J_x(s) J_x(0) \rangle ds. \tag{8}$$

The interactions between particles were modeled using the Weeks-Chandler-Anderson modification of the Lennard-Jones potential (if r is the distance between two particles, $\phi(r) = -4\varepsilon[(\sigma/r)^6 - (\sigma/r)^{12}] + \varepsilon$ for $r \le 2^{1/6}\sigma$ and 0 otherwise). The two types of particles differ only in the way they couple to the color field (half of the particle is assigned a charge $z_i = 1$ while the other half is assigned $z_i = -1$). In other words, there is no Coulombic interaction between particles. Throughout this work, we use a reduced system of units [34] in which the units of length, mass, and energy are σ, m, and ε. We carried out simulations of the bulk as well as of the confined fluid. We choose to confine the fluid in cylindrical nanopores of a radius R, whose section is perpendicular to the x axis (and thus to the applied field). The interaction between the particles and the confining wall is defined as $\phi_{\text{wf}}(r) = \varepsilon\{\sigma/[R - \sqrt{(y^2+z^2)}]\}^{12}$ if $[R - \sqrt{(y^2+z^2)}] \le 2^{1/6}\sigma$ and 0 otherwise. As always, there is some ambiguity in defining the effective radius and thus the effective volume for the confined system. We choose to define the effective radius by $R_{\text{eff}} = R - 1$. All simulations for the bulk and the confined systems were carried out at constant number density $n = 0.84$ and constant temperature $T = 0.75$. We used systems of $N = 256$ particles for simulations of the bulk and of the narrower pores (effective radii of 2.5, 3, and 4) and $N = 512$ particles for the larger pores (effective radii of 6 and 7). We integrate the equations of motion with a Runge-Kutta integrator and a time step of 2×10^{-3}. The parameter for the configurational thermostat Q_η is set to 5×10^5 as in Ref. [30]. Periodic boundary conditions are applied to the system in the three directions of space for the simulations of the bulk and in the x direction only for the simulations of the confined fluid. Each system was started off by inserting the particles at random positions within the desired volume. The systems were first equilibrated for 10^6 time steps. During subsequent simulation runs, we selected 10 000 equilibrium configurations for each system at intervals of 2–3 time units. From each of these configurations, we can define three other equilibrium configurations: (i) by reversing the sign of the momenta of all particles (also termed time-reversal mapping [10]), (ii) by mirror symmetry (reversing the sign of x and p_x for all particles), and (iii) by applying both the time-reversal mapping and the mirror symmetry. The 40 000 configurations so obtained were the starting points for the nonequilibrium trajectories. In addition to being more efficient, this

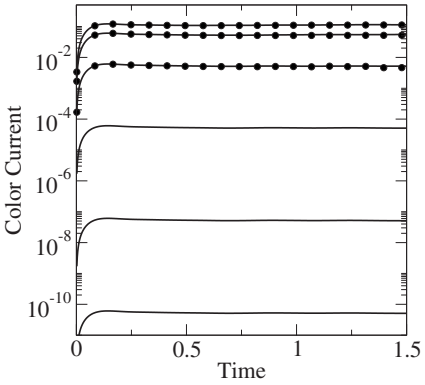

FIG. 1. Bulk. TTCF estimate (line) of the color current for an applied field of 2, 1, 0.1, 10^{-3}, 10^{-6}, and 10^{-9} (from top to bottom). Direct averages (circles) are shown for fields of 2, 1, and 0.1.

procedure also ensured that $\langle J_x(0)\rangle$ was exactly zero.

We begin by assessing the reliability of the TTCF approach for the bulk. We summarize in Fig. 1 the results obtained for the color current using the TTCF formalism. The TTCF approach allows for an accurate determination of the color current, in the transient regime as well as in the steady state, over the whole range of color fields studied from 10^{-9} to 2. This is a definite improvement over the conventional NEMD method, which is unable to give a reliable estimate for the color current for fields below 10^{-3}. We will illustrate this point later in this paper on the example of the confined fluid.

There are essentially two ways of assessing the validity of the TTCF approach developed in this work. First, when the color field tends toward zero, the value for the color conductivity given by the TTCF approach [Eq. (8)] should exhibit a plateau and converge toward the Green-Kubo estimate for the conductivity. This is because the system enters the linear response regime as the color field decreases. We carry out equilibrium molecular dynamics simulations in the *NVT* ensemble over 2000 time units and estimate the color conductivity according to the following Green-Kubo expression:

$$\sigma = \frac{V}{k_B T}\int_0^\infty \langle J_x(s)J_x(0)\rangle ds. \tag{9}$$

We find a Green-Kubo estimate for the color conductivity of 0.048 ± 0.005. Using the TTCF [Eq. (8)], we find that the color conductivity reaches a plateau of 0.051 ± 0.005 for fields below 10^{-3}. The excellent agreement between the Green-Kubo and the TTCF estimates demonstrates the reliability of the TTCF approach. Second, for very high fields, the direct steady-state average should coincide with the TTCF estimates. This is because (i) the TTCF formalism gives an exact relation between the nonlinear steady-state response and the transient-time correlation function and (ii) for a strong enough field, the signal-to-noise ratio is large enough for steady-state averages to be measured. The direct steady-state average can be measured during the course of the NEMD simulations as

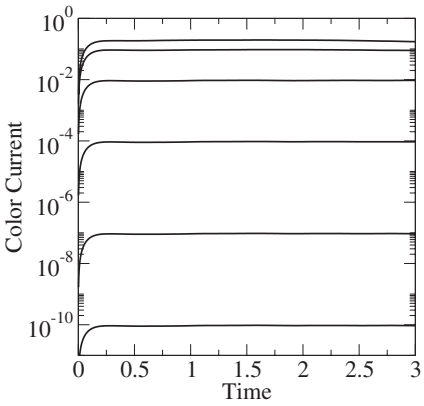

FIG. 2. Cylindrical nanopore with an effective radius of 4. Color current against the color field for an applied field of 2, 1, 0.1, 10^{-3}, 10^{-6}, and 10^{-9} (from top to bottom).

$$\langle J_x(t)\rangle = \frac{\sum_{i=1}^{N_t} J_{x,i}(t)}{N_t}, \tag{10}$$

where N_t=40 000 is the number of nonequilibrium trajectories considered. As shown in Fig. 1, the direct steady-state average and the TTCF estimate for the color current are in excellent agreement for the stronger fields, thereby demonstrating the reliability of the TTCF approach under far-from-equilibrium conditions.

We extend the TTCF approach to systems confined in cylindrical nanopores and subjected to a color field. We plot in Fig. 2 the TTCF results obtained for the color current when the fluid is confined in a pore of R_{eff}=4. The TTCF approach allows us to obtain reliable estimates of the color current for a confined fluid, both in the transient regime and in the steady state, over the whole range of fields we studied, i.e., from 10^{-9} to 2. We plot in Fig. 3 TTCF estimates of the color conductivity for a fluid confined in a pore of R_{eff}=2.5. As observed for the bulk for strong applied fields, we find that the TTCF estimate and the direct average give results in excellent agreement (e.g., for a field of 1 in Fig. 3). Simi-

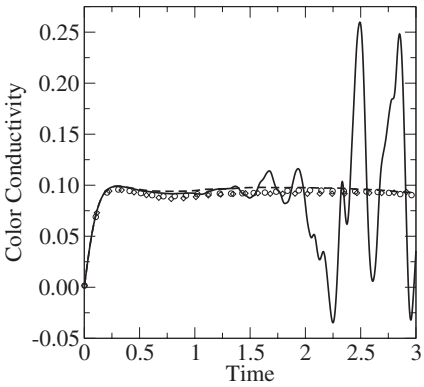

FIG. 3. Cylindrical nanopore with an effective radius of 2.5. Color conductivity against the color field for an applied field of 1 (direct average, dashed line; TTCF estimate, circles) and of 10^{-3} (direct average, solid line; TTCF estimate, diamonds).

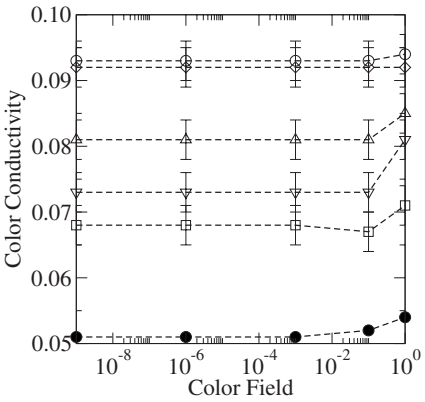

FIG. 4. Color conductivity as a function of the applied color field: bulk (filled circles) and cylindrical nanopores with an effective radius of 6 (squares), 5 (down triangles), 4 (up triangles), 3 (diamonds), and 2.5 (open circles).

larly, for a weaker field (below 0.001), the signal-to-noise ratio becomes too small and carrying out a direct average over the 40 000 NEMD trajectories leads to a very noisy and unreliable estimate for the color conductivity (see, e.g., the result for a field of 0.001 in Fig. 3).

We finally summarize the results obtained for all systems (bulk and confined) in Fig. 4. Confining the fluid in a nanopore, with an effective radius larger than or equal to 2.5, systematically results in an increased conductivity with respect to the bulk. The conductivity strongly depends on the effective radius of the cylindrical nanopore. For $R_{\mathrm{eff}}>3$, the conductivity increases as the effective diameter of the pore decreases. We obtain similar values for the conductivity for the two narrower pores, $R_{\mathrm{eff}}=2.5$ and 3. The maximum conductivity—roughly twice that of the bulk—will be obtained for an effective diameter of about 2.5. When the fluid is confined in a narrower pore, $R_{\mathrm{eff}}\leq 2$, there is not enough room for the particles of different colors to move in opposite directions. As a result, for $R_{\mathrm{eff}}\leq 2$, we find that the current, and hence the conductivity, vanishes in the steady state.

In this work, using the TTCF, we showed how NEMD simulations can be extended to study the conductivity of a model liquid confined in a cylindrical nanopore subjected to a realistic field. Our results provide a full picture of the dependence of conductivity on the applied field and on the effective diameter of the nanopore. Our results show that a nanoscopic confinement enhances the conductivity since the conductivity steadily increases—up to twice the value evaluated for the bulk—as the effective radius of the pore decreases. The method developed in this work can be readily applied to realistic models for electrolytes for any kind of pore geometry.

[1] J. Piasecki, R. J. Allen, and J. P. Hansen, Phys. Rev. E **70**, 021105 (2004).
[2] K.-Y. Chan, Y. W. Tang, and I. Szalai, Mol. Simul. **30**, 81 (2004).
[3] C. Ho, R. Qiao, J. B. Heng, A. Chatterjee, R. J. Timp, N. R. Aluru, and G. Timp, Proc. Natl. Acad. Sci. U.S.A. **102**, 10445 (2005).
[4] L. Yang and S. Garde, J. Chem. Phys. **126**, 084706 (2007).
[5] J. Petravic and J. Delhommelle, J. Chem. Phys. **118**, 7477 (2003).
[6] J. Petravic and J. Delhommelle, J. Chem. Phys. **119**, 8511 (2003).
[7] W. M. Visscher, Phys. Rev. A **10**, 2461 (1974).
[8] J. W. Dufty and M. J. Lidenfeld, J. Stat. Phys. **20**, 259 (1979).
[9] E. G. D. Cohen, Physica A **118**, 17 (1983).
[10] D. J. Evans and G. P. Morriss, *Statistical Mechanics of Nonequilibrium Liquids* (Academic, London, 1990).
[11] G. P. Morriss and D. J. Evans, Phys. Rev. A **39**, 6335 (1989).
[12] I. Borzsak, P. T. Cummings, and D. J. Evans, Mol. Phys. **100**, 2735 (2002).
[13] J. Petravic and P. Harrowell, Phys. Rev. E **71**, 061201 (2005).
[14] J. Delhommelle and P. T. Cummings, Phys. Rev. B **72**, 172201 (2005).
[15] B. D. Todd, Phys. Rev. E **56**, 6723 (1997).
[16] G. Pan, J. F. Ely, C. McCabe, and D. J. Isbister, J. Chem. Phys. **122**, 094114 (2005).
[17] J. Delhommelle, P. T. Cummings, and J. Petravic, J. Chem. Phys. **123**, 114505 (2005).
[18] J. P. Dzubiella, G. P. Hoffmann, and H. Lowen, Phys. Rev. E **65**, 021402 (2002).
[19] J. Delhommelle and D. J. Evans, J. Chem. Phys. **114**, 6229 (2001).
[20] J. Delhommelle and D. J. Evans, J. Chem. Phys. **114**, 6236 (2001).
[21] K. P. Travis and K. E. Gubbins, J. Chem. Phys. **112**, 1984 (2000).
[22] J. Delhommelle, J. Petravic, and D. J. Evans, Phys. Rev. E **68**, 031201 (2003).
[23] J. Delhommelle, J. Petravic, and D. J. Evans, J. Chem. Phys. **119**, 11005 (2003).
[24] J. Delhommelle, Phys. Rev. E **71**, 016705 (2005).
[25] J. Delhommelle, Phys. Rev. B **69**, 144117 (2004).
[26] J. Delhommelle and D. J. Evans, J. Chem. Phys. **115**, 43 (2001).
[27] J. Delhommelle and D. J. Evans, Mol. Phys. **99**, 1825 (2001).
[28] L. Lue, O. G. Jepps, J. Delhommelle, and D. J. Evans, Mol. Phys. **100**, 2387 (2002).
[29] J. Delhommelle and D. J. Evans, J. Chem. Phys. **117**, 6016 (2002).
[30] C. Braga and K. P. Travis, J. Chem. Phys. **123**, 134101 (2005).
[31] J. Delhommelle and J. Petravic, J. Chem. Phys. **118**, 2783 (2003).
[32] H. H. Rugh, Phys. Rev. Lett. **78**, 772 (1997).
[33] O. G. Jepps, G. Ayton, and D. J. Evans, Phys. Rev. E **62**, 4757 (2000).
[34] M. P. Allen and D. J. Tildesley, *Computer Simulation of Liquids* (Clarendon, Oxford, 1987).